Hindawi
Journal of Nanomaterials
Volume 2021, Article ID 6696995, 11 pages
https://doi.org/10.1155/2021/6696995

Research Article

Highly Effective Degradation of Nitrophenols by Biometal Nanoparticles Synthesized using *Caulis Spatholobi* Extract

Van Thuan Le,[1,2] Van-Cuong Nguyen,[3] Xuan-Thang Cao,[3] Tan Phat Chau,[4] Thi Dung Nguyen,[5] Thi Lan-Huong Nguyen,[6] and Van-Dat Doan[3]

[1]*Center for Advanced Chemistry, Institute of Research and Development, Duy Tan University, 03 Quang Trung, Da Nang 550000, Vietnam*
[2]*The Faculty of Environmental and Chemical Engineering, Duy Tan University, 03 Quang Trung, Da Nang 550000, Vietnam*
[3]*Faculty of Chemical Engineering, Industrial University of Ho Chi Minh City, 700000 Ho Chi Minh City, Vietnam*
[4]*Institute of Applied Science & Technology, Van Lang University, Ho Chi Minh City 700000, Vietnam*
[5]*Division of Food Biotechnology, Biotechnology Center of Ho Chi Minh City, Ho Chi Minh City 700000, Vietnam*
[6]*Institute of Biotechnology and Food Technology, Industrial University of Ho Chi Minh City, Ho Chi Minh City 700000, Vietnam*

Correspondence should be addressed to Van-Dat Doan; doanvandat@iuh.edu.vn

Received 26 October 2020; Revised 5 December 2020; Accepted 8 March 2021; Published 22 March 2021

Academic Editor: Hassan Karimi-Maleh

The green biosynthesis of metal nanoparticles (MNPs) has been proved to have many advantages over other methods due to its simplicity, large-scale production, ecofriendly approach, and high catalytic efficiency. This work describes a single-step technique for green synthesis of colloidal silver (AgNPs) and gold nanoparticles (AuNPs) using the extract from *Caulis Spatholobi* stems. Ultraviolet-visible spectroscopy measurements were used to optimize the main synthesis factors, including metal ion concentration, reaction time, and reaction temperature via surface plasmon resonance phenomenon. Fourier-transform infrared spectroscopy showed the possible functional groups responsible for reducing and stabilizing the synthesized MNPs. The powder X-ray diffraction and selected area electron diffraction analysis confirmed the crystalline nature of the biosynthesized MNPs. High-resolution transmission electron microscopy revealed the spherical shape of MNPs with an average size of 10-20 nm. The obtained MNPs also exhibited the enhanced catalytic activity in the reduction of 2-nitrophenol and 3-nitrophenol.

1. Introduction

Noble metal nanoparticles (MNPs) are considered as an important class in the next generation of nanomaterials for catalytic degradation of organic pollutants due to their extraordinary large surface area and great dispersion in aqueous solutions [1]. Among them, silver and gold nanoparticles (AgNPs and AuNPs) have received great attention for their applicability in many fields, especially in catalysis [2]. Therefore, many different approaches for the synthesis of AgNPs and AuNPs have been developed, including physical, chemical, and biological methods [3]. However, the drawbacks of physical and chemical methods may be the low production efficiency, requirement of expensive equipment, usage of toxic reductants, and the long-time reaction, which might affect the cost of obtained products [4]. Compared with the traditional chemical methods, biogenic synthesis of AgNPs and AuNPs using herbal plant extracts is an ecofriendly solution due to its sustainable nature and environmentally benign [5]. The first use of plant extract for the synthesis of MNPs was recorded by Gardea-Torresdey et al. in 2003 [6]. It was reported that the formation of MNPs using plant extract from *Alfalfa* sprouts could be accomplished under normal conditions in a short period of contact time. Since then, extracts from different parts of plants such as leaves [7–10], flowers [11–14], stems [15–18], latex [19–21], roots [22, 23], and seeds [24–26] are intensively utilized for MNP synthesis. The organic molecules in plant extracts, including

phenolic compounds, polysaccharides, terpenoids, alkaloids, flavonoids, and amino acids, can act simultaneously as reducing and stabilizing agents [3].

Caulis Spatholobi (CS) is a herbal species belonging to the Fabaceae family that can be easily found in the northern mountainous region of Vietnam and China at altitudes not exceeding 1600 m along the rivers and streams [27]. In traditional medicine, CS stem is usually used to improve blood circulation and becalm dysmenorrhea, paralysis, arthralgia, and anaemia. Recently, it is reported that the extract of CS has been a novel tumour cell-induced platelet aggregation inhibitor, which can significantly restrain the metastasis of colorectal cancer [28]. The main chemical constituents of CS include phenolic acids, isoflavones, flavanoles, flavanones, flavanonol, and phytosterols [29], which have great potential applications as reducing and stabilizing agents for the synthesis of MNPs. To our knowledge, up to now, there is no report in the literature about using CS extract for the synthesis of AgNPs and AuNPs.

Concerning catalytic activity, recent studies show that AgNPs and AuNPs possess a good catalytic performance in the transformation of toxic nitrophenolic compounds into useful aminophenols [5]. Among various derivatives of nitrophenols, 2-nitrophenol (2-NP) and 3-nitrophenol (3-NP) are often found in the textile industrial wastewater as well as the agricultural [30]. Sodium borohydride ($NaBH_4$) is usually used as a typical reductant for the degradation of organic pollutants. However, $NaBH_4$ has almost no reducing power for these nitrophenols without a catalyst. Kariuki et al. reported that the reduction reaction of nitrophenols using $NaBH_4$ remained unchanged in the absence of a catalyst because of the high kinetic barrier between the mutually repelling negative nitrophenol ions and BH_4^- [31]. Meanwhile, the reaction became kinetically favorable in the presence of AgNPs and AuNPs. The activation energy can be quickly lowered by using AgNPs and AuNPs via changing the path of electron transfer [32]. In this context, finding ecofriendly biosynthesized AgNPs and AuNPs with enhanced catalytic performance is significantly important and is the main task for the research community.

Herein, we report a single-step biosynthesis of AgNPs and AuNPs using the herbal plant extract of CS as a reducing and capping agent. Synthesis parameters affecting the size of MNPs such as reaction time, metal ion concentration, and reaction temperature were optimized. The morphology, structure, and chemical composition of the biosynthesized MNPs were explored in detail. The produced AgNPs and AuNPs were found to be efficient catalysts in reducing 2-NP and 3-NP to respective 2-aminophenol (2-AP) and 3-aminophenol (3-AP) by $NaBH_4$.

2. Material and Methods

2.1. Materials and Chemicals. Silver nitrate ($AgNO_3$) and hydrogen tetrachloroaurate (III) hydrate ($HAuCl_4{\cdot}3H_2O$) were of high purity supplied by Acros (Belgium) and used without any purification. Sodium tetrahydridoborate ($NaBH_4$), 2-nitrophenol ($C_6H_5NO_3$), and 3-nitrophenol ($C_6H_5NO_3$) were purchased from Merck (India). CS stems were collected from mountainous Lang Son province, Vietnam, with the location at coordinates 21.8537°N, 106.7615°E. The fresh CS stems were washed thoroughly with tap water to remove all the dirt and then rinsed with distilled water. Next, the stems were further sliced into pieces with a width of about 2 cm and dried up at 50°C in the oven for one week until its humility reached about 8%. The dried CS stems were crushed into powder by a blender for obtaining extract.

2.2. Preparation of CS Extract. The CS powder (5 g) was added to 300 mL of distilled water and boiled over low heat with a reflux condenser for 1 h. The obtained mixture was cooled down to room temperature and filtered with Whatman filter paper No. 1 to eliminate all suspended solids. The CS extract was stored at 4-10°C in a refrigerator before use for the MNP synthesis.

2.3. Synthesis of CS-AgNPs and CS-AuNPs. The synthesis of biogenic AgNPs and AuNPs was performed by mixing in the dark 10 mL of CS extract with 10 mL of $AgNO_3$ or $HAuCl_4$ solutions under vigorous stirring. The success of the synthesis process was observed via a color change of the solution by the surface plasmon resonance (SPR) phenomenon after reactions were completed [33]. Various synthesis factors, including metal ion concentration (0.5-2 mmol/L), reaction time (10-50 min), and reaction temperature (60-100°C), were optimized using UV-Vis spectrometry measurements. The SPR peaks of about 420 nm and 540 nm were characterized for AgNPs and AuNPs, respectively [34]. The biosynthesized MNPs were separated by an ultracentrifuge and dried up at 80°C in an oven for further catalytic application. The procedure for the biosynthesis of CS-AgNPs and CS-AuNPs and their application are illustrated in Figure 1.

2.4. Characterization of MNPs. The presence of functional groups in the dried CS extract and biosynthesized CS-AgNPs and CS-AuNPs was monitored by Fourier transform infrared spectroscopy (FTIR) within the range of 4000-500 cm^{-1} on an Equinox 55 FTIR spectrometer (Germany). The crystalline nature, crystal size, and purity of MNPs were analyzed by a powder X-ray diffraction (XRD) method on a Shimadzu 6100 X-ray diffractometer (Japan) using CuKα radiation ($\lambda = 1.5406$ Å) at a voltage of 40 kV, current of 30 mA, scanning speed of 3.0°/min, and step size of 0.02° in the 2θ range of 10-80°. The shape and size of the MNPs were examined by high-resolution transmission electron microscopy (HR-TEM) on a JEOL JEM-2100 (Japan) at an operating voltage of 200 kV. The crystalline nature was confirmed by the selected area electron diffraction pattern (SAED). The field-emission scanning electron microscopy (FE-SEM) images were recorded on a Hitachi S-4800 (Japan) at an accelerating voltage of 10 kV for the examination of CS-AgNPs and CS-AuNPs after centrifugation. The chemical elemental composition of MNPs was analyzed using energy-dispersive X-ray spectroscopy (EDX) on a Horiba EMAX Energy EX-400 analyzer (Japan). The thermal behavior of CS-AgNPs and CS-AuNPs was evaluated by combining thermogravimetric analysis (TGA) and differential thermal analysis (DTA) using a Mettler Toledo

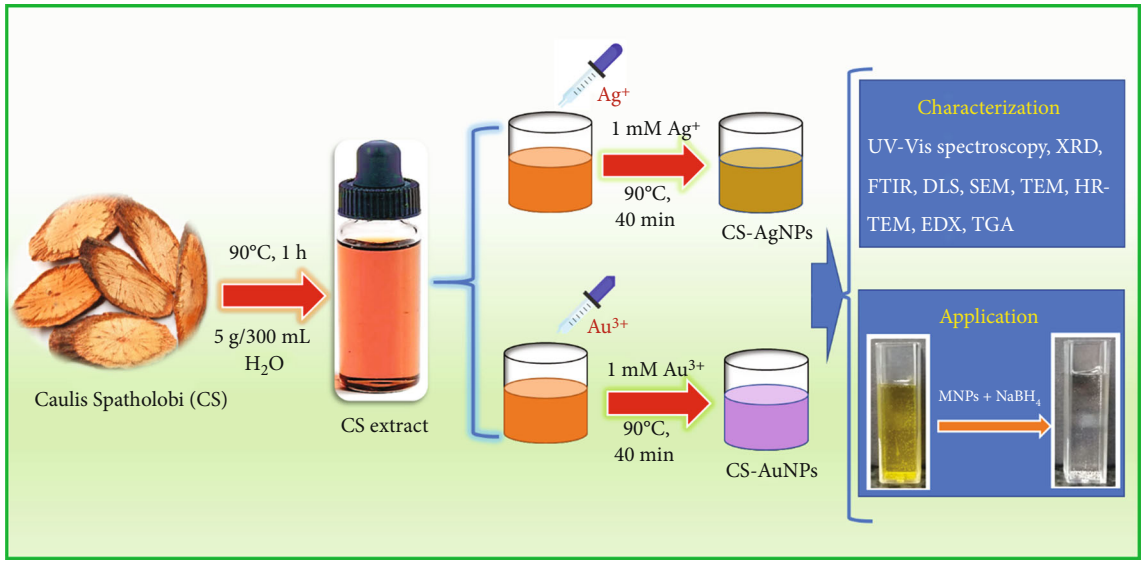

Figure 1: Schematic illustration for the biosynthesis of CS-AgNPs and CS-AuNPs and their application.

TGA/DSC 3+ (Switzerland). Finally, the dynamic size of the nanoparticles was examined using the dynamic light scattering (DLS) method conducted on a Horiba SZ-100 (Japan).

2.5. Catalytic Degradation Experiments. The catalytic activity of the biosynthesized MNPs for the 2-NP or 3-NP reduction with $NaBH_4$ was analyzed at room temperature. Briefly, a freshly prepared solution of $NaBH_4$ (0.5 mL of 0.1 mol/L) was added into a cuvette containing 2-NP or 3-NP (2.5 mL, 0.1 mmol/L), followed by adding dried MNPs (3 mg). After the nitrophenols were completely reduced, the MNPs were centrifuged and washed thoroughly with distilled water and then ethanol for reuse. The kinetics of the catalytic degradation process was evaluated by UV-Vis spectroscopy in the wavelength range of 250-700 nm. The concentration of $NaBH_4$ was used in excess over the concentration of the nitrophenols so that the degradation process could be considered as a pseudo-first-order reaction [35]. The reaction rate constant k was determined after plotting a linear regression of ln (A_t) over reaction time t, where A_t is the optical density of the mixture at the time t.

3. Results and Discussions

3.1. Optimization of Biosynthesis Conditions. The MNPs biosynthesized by plant extracts are mostly polydispersed because of the different nature of organic molecules, which act as reducing agents [3]. Herein, the size can be optimized by alerting reaction parameters. In this context, three main reaction parameters, including the concentration of metal ions, reaction time, and reaction temperature, were investigated.

To study the effect of metal ion concentration, the concentrations of $AgNO_3$ and $HAuCl_4$ solutions were varied from 0.5 to 2.0 mmol/L, while fixing the reaction time and reaction temperature at 40 min and 90°C, respectively. It can be seen from Figures 2(a) and 2(a′) that the concentration of metal ions significantly affected not only the size of the formed MNPs but also the stability of the resulting suspension. In fact, the increase in metal ion concentration led to the higher yield of the nanoparticles. No shift of maximum wavelength was observed. However, at the metal ion concentration greater than 1.5 mmol/L, the UV-Vis curves were not very smooth, which could be related to the aggregation of MNPs after a short time.

The reaction time for the biosynthesis of MNPs was optimized by recording UV-Vis measurements every 10 min while the two other parameters (90°C and 1.0 mmol/L of metal ion) were maintained. For both cases, the reaction time of 40 min could be chosen as optimal to perform further synthesis since no higher yield of nanoparticles was obtained at a longer reaction time (Figures 2(b) and 2(b′)).

Finally, the effect of reaction temperature on the formation of AgNPs and AuNPs was studied in the range of 50-100°C, as shown in Figures 2(c) and 2(c′), respectively. The obtained results indicated that the optimal reaction temperature could be chosen at 90°C for synthesizing both CS-AgNPs and CS-AuNPs. In the case of CS-AuNPs, the increase in temperature over 90°C led to a formation of larger size MNPs, while the number of nanocrystals was reduced, causing a reduction of their optical density. For CS-AgNPs, the low stable suspension was observed at reaction temperature over 90°C with the proof of no smooth UV-Vis curve. This phenomenon could be related to the fact that at higher temperatures, the formed nanoparticles possessed the greater kinetic energy, increasing the probability of collisions, which resulted in partial coagulation of MNPs.

3.2. Characterization of Biogenic MNPs. The XRD patterns of the biosynthesized CS-AgNP and CS-AuNP samples obtained at optimal conditions are presented in Figure 3(a). The XRD pattern of CS-AgNPs shows four characteristic

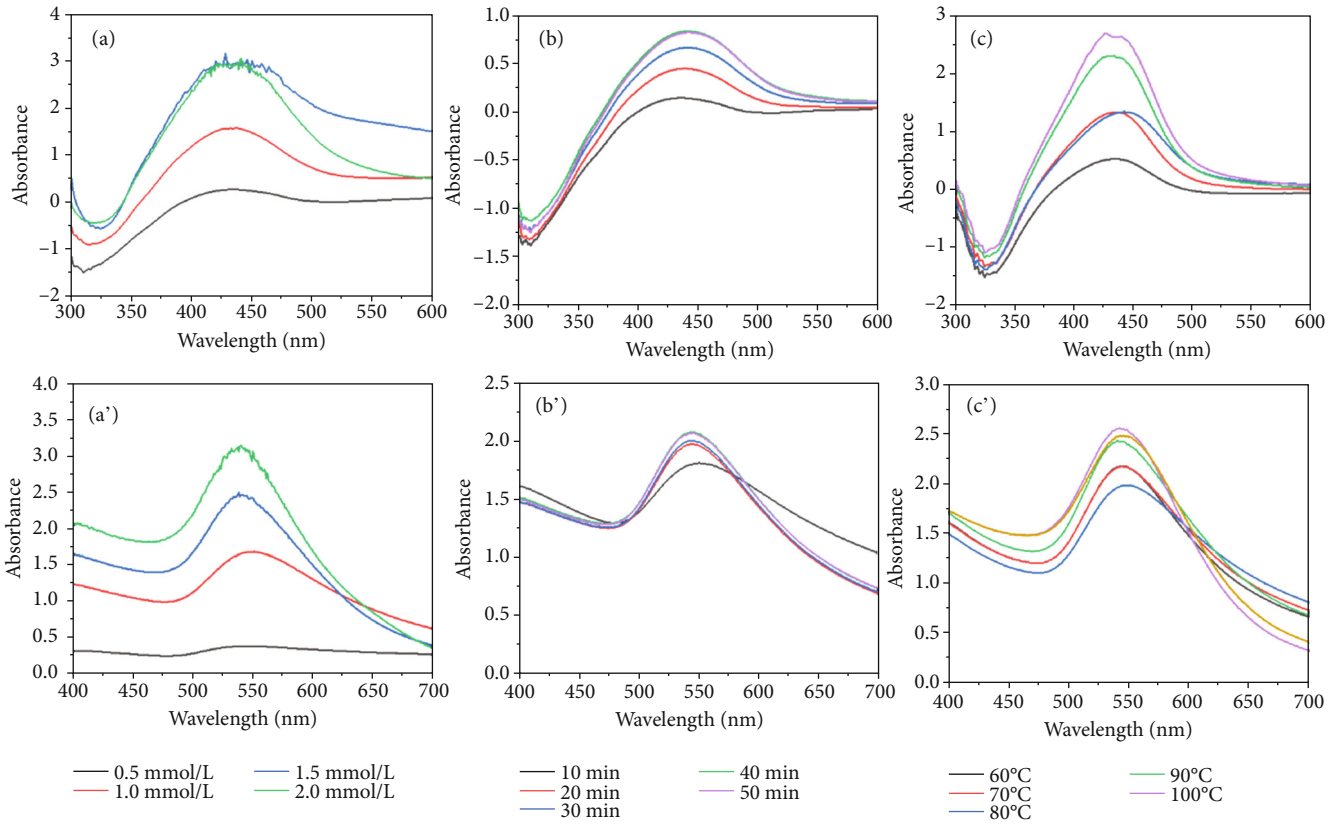

Figure 2: UV-Vis spectra of CS-AgNPs (a–c) and CS-AuNPs (a′–c′) solutions at different metal ion concentrations (a, a′), reaction time (b, b′), and temperatures (c, c′).

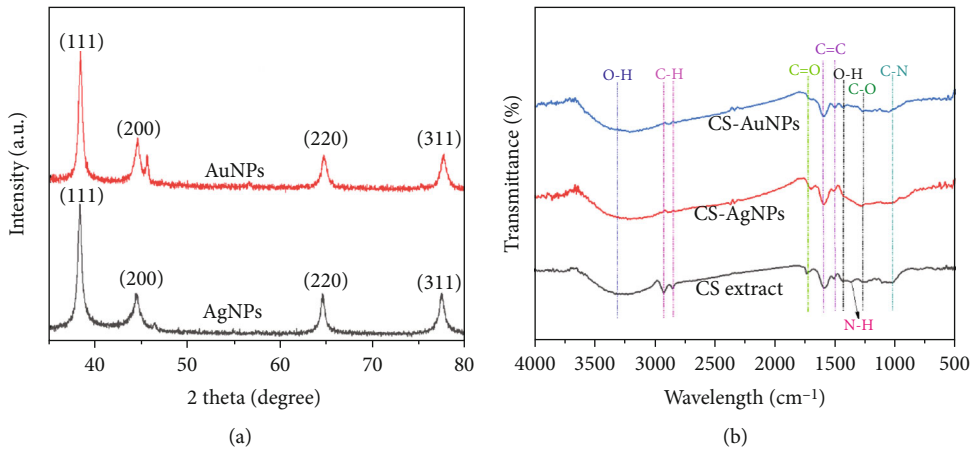

Figure 3: (a) XRD patterns and (b) FTIR spectra of CS-AgNPs and CS-AuNPs.

peaks of (111), (200), (220), and (311) planes diffracted at the corresponding 2θ angles of 38.21°, 44.35°, 64.56°, and 77.48°, respectively. According to the ICDD PDF No. 00-004-0783, AgNPs with the face-centred cubic (FCB) were successfully synthesized [36]. A similar result was also recorded for CS-AuNPs. The typical peaks at 38.29° (111), 44.44° (200), 64.73° (220), and 77.63° (311) assigned to the FCB structure of gold (ICDD PDF No. 00-004-0784) were detected [37]. In both two cases, the CS-AgNPs and CS-AuNPs exhibited the highest diffraction peak of about 38.2°, revealing that their crystals had been grown preferably along the (111) plane. The presence of only above-mentioned sharp peaks in the XRD patterns confirmed a high crystallinity and crystalline purity of the prepared MNPs. The average crystal size of CS-AgNPs and CS-AuNPs, according to the Debye-Scherrer equation, was calculated to be 15.05 and 16.40 nm, respectively.

The FTIR spectra of the dried CS extract, CS-AgNPs, and CS-AuNPs are shown in Figure 3(b). The similarity for absorption bands in the FTIR spectra of all samples indicated

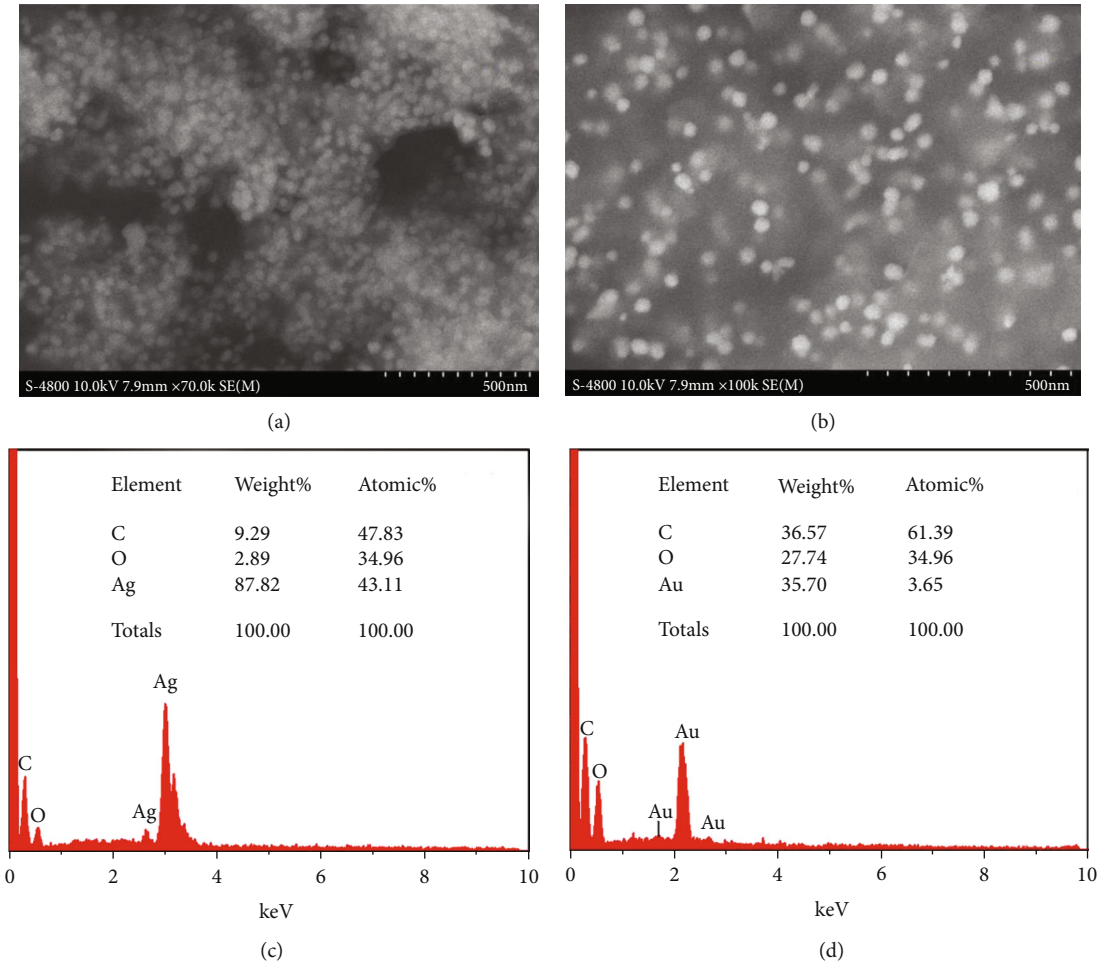

Figure 4: SEM images and EDX spectra for CS-AgNPs (a, c) and CP-AuNPs (b, d).

the presence of the same covalent bonds. The broad band centred at 3229 cm^{-1} is related to the stretching vibrations of O–H groups [4] in phenolic acids, flavanoles, flavanonol, and phytosterols present in the CS extract, as reported in [29]. The peaks at 2928 and 2855 cm^{-1} are allocated to C–H stretching vibrations of $–CH_3$ and $–CH_2$- bonds [38]. The band at 1740 cm^{-1} may be attributed to the ketone stretch C=O of isoflavones and flavanones in the CS extract [35]. The peak at 1592 cm^{-1} is assigned to –C=C– bond stretching of aromatic rings [39]. The peaks that appeared at 1242 and 1028 cm^{-1} are attributed to the C–O and C–N band stretching of ether and amine groups, respectively [40]. It is noteworthy that the peak at 1279 cm^{-1} characteristic for amine groups was observed only in the spectra of dried CS extract, suggesting the involvement of those groups in the bioreduction/capping of MNPs, along with polyol groups [41].

The SEM images and EDX spectra of the biosynthesized MNPs are shown in Figure 4. As seen in Figures 4(a) and 4(b), both CS-AgNPs and CS-AuNPs are mostly spherical and uniformly distributed. The EDX spectrum of CS-AgNPs (Figure 4(c)) demonstrates the presence of strong peaks at 2.72 and 2.98 keV that proved the existence of the silver element. The EDX spectrum of CS-AuNPs (Figure 4(c)) also shows the appearance of the gold element with characteristic peaks at 1.74 and 2.165 keV. Besides, the peaks related to carbon (0.4 keV) and oxygen (0.55 keV) were also detected, confirming the presence of organic matter, which acted as a capping agent. It is evident that the average content of silver (87.82 w%) is much greater than that of gold (35.70 w%); subsequently, the average total content of carbon and oxygen in CS-AuNPs (64.31 w%) is superior to that of CS-AgNPs (12.18 w%). This can be due to the gold ion with a greater charge that can attract more organic molecules in CS extract in the synthesis process than silver ion. No strange peaks of other elements were observed, once again confirming the high purity of the biosynthesized MNPs.

The TEM images, SAED patterns, and DLS measurements of MNPs in the colloidal solution form are shown in Figure 5. It is clear from Figures 5(a) and 5(a′) that the CS-AgNPs and CS-AuNPs are mostly spherical in shape and dispersed well in the colloidal solution without any coagulation. The average size of CS-AgNPs and CS-AuNPs determined by TEM images is about 16.4 nm and 18.2 nm, respectively. The crystalline nature of CS-AgNPs and CS-AuNPs in a cubic crystal form is confirmed by the bright circular rings in SAED patterns (Figures 5(b) and 5(b′), respectively). The lattice fringes of CS-AgNPs and CS-AuNPs between (111) planes have d-spacing of 0.22 and 0.26 nm, respectively.

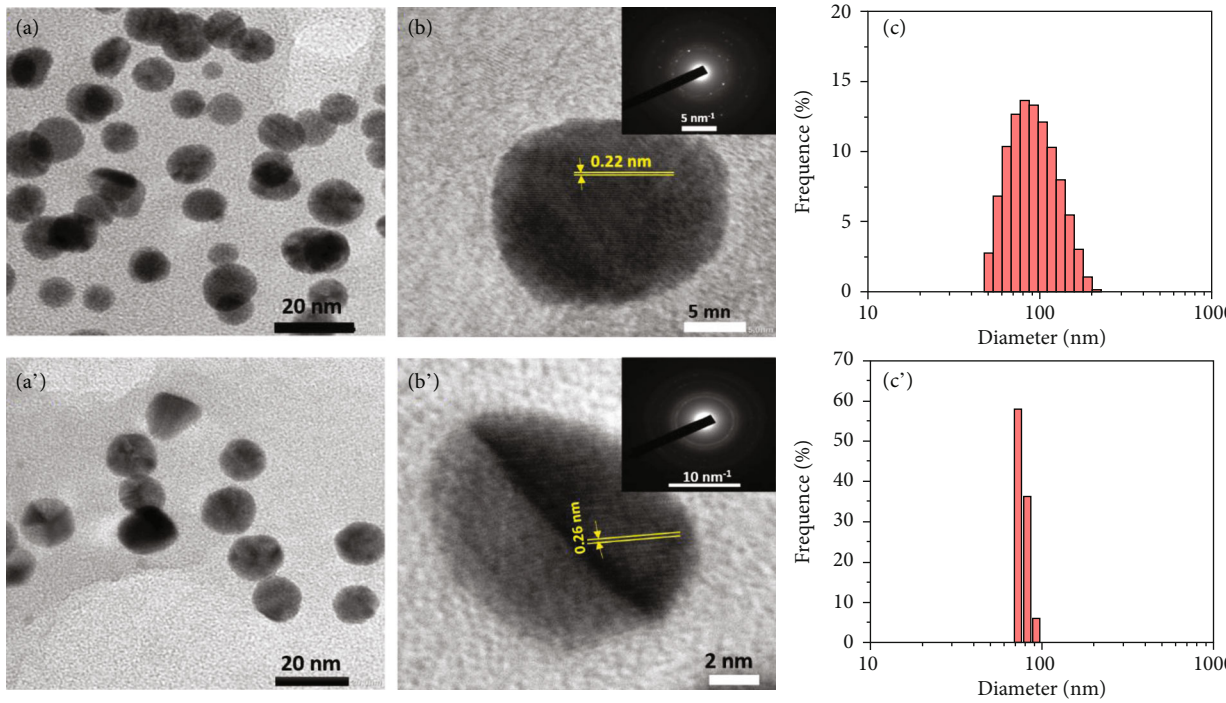

Figure 5: TEM (a, a′), HR-TEM (b, b′) images, SAED (inset of b and b′), and DLS (c, c′) of CS-AgNPs (a–c) and CS-AuNPs (a′–c′).

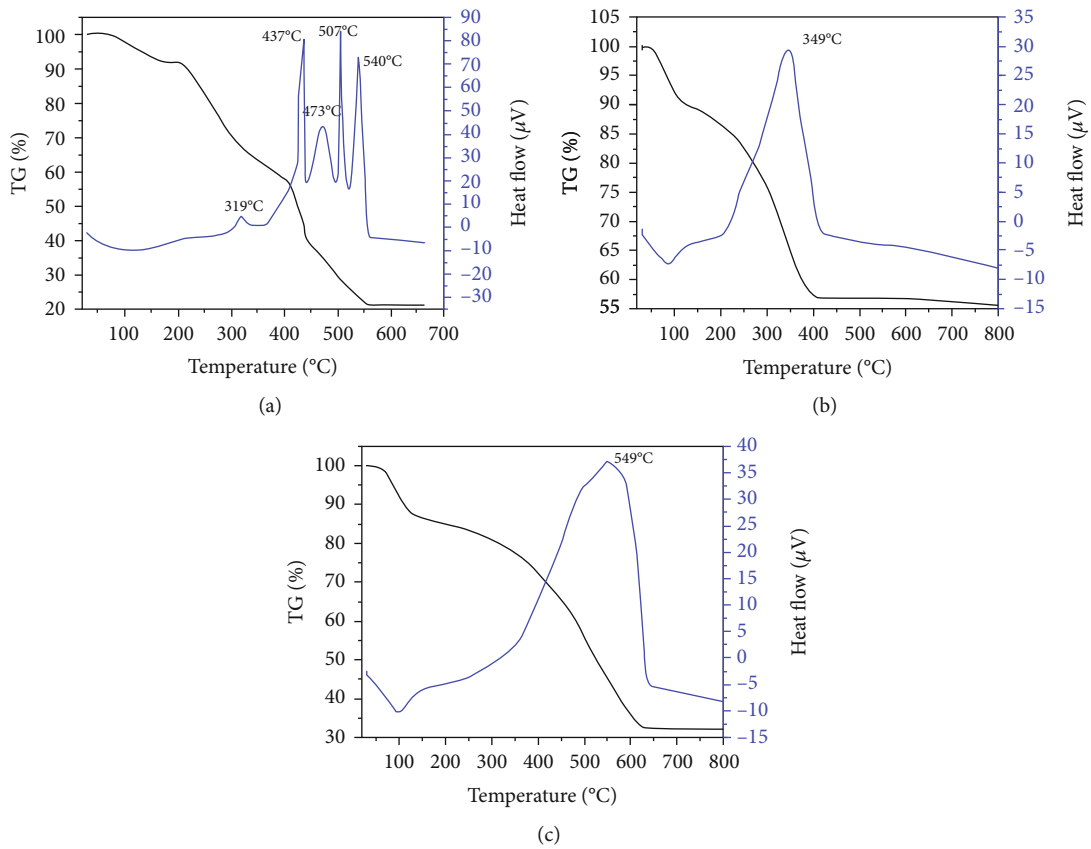

Figure 6: TGA of CS extract (a), CS-AgNPs (b), and CS-AuNPs (c).

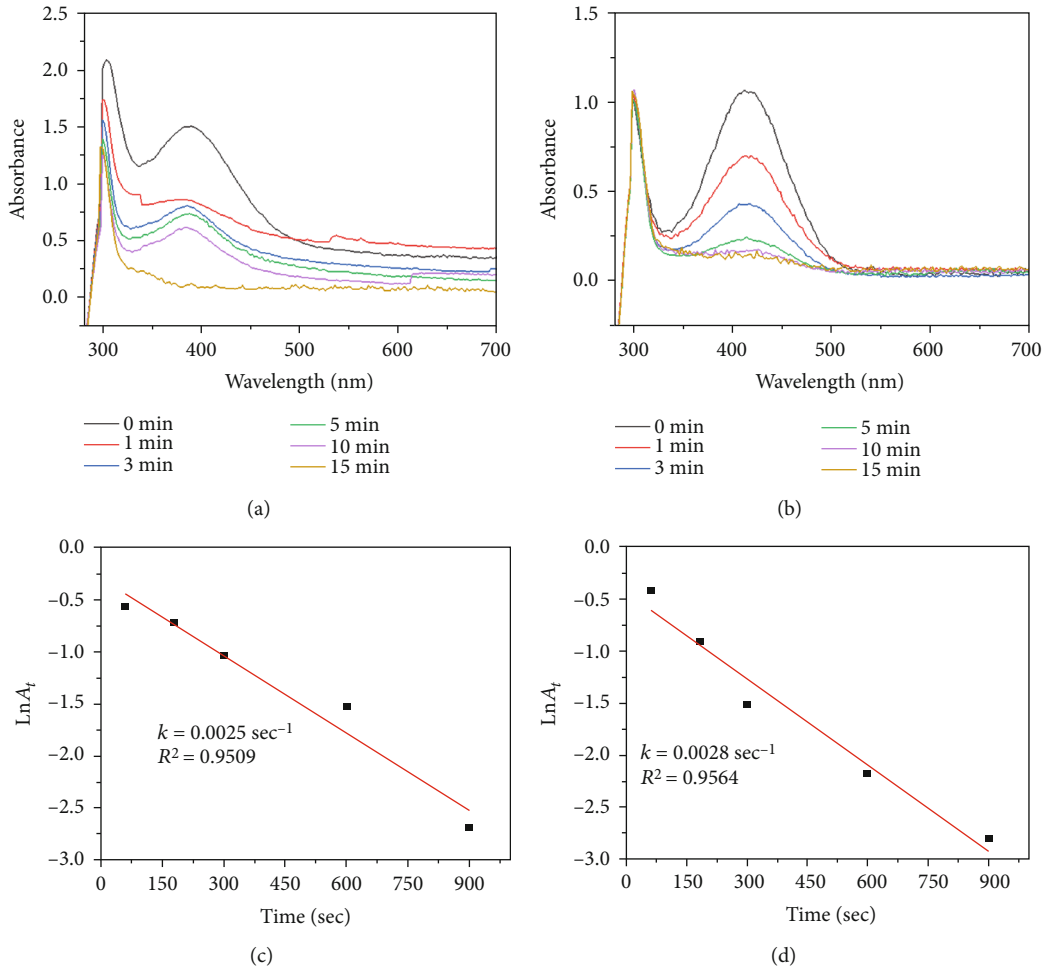

Figure 7: UV-Vis spectra (a, b) and first-order kinetics (c, d) for degradation of 2-NP by $NaBH_4$ in the presence of CS-AgNPs (a, c) and CS-AuNPs (b, d).

According to the particle size distribution diagrams of MNPs presented in Figures 5(c) and 5(c′), the hydrodynamic diameters of CS-AgNPs and CS-AuNPs are about 66.3 and 71.2 nm, respectively. It should be noted that the quite bigger particle size obtained by DLS analysis compared to those by the TEM method is usually observed for colloidal solutions. It is due to DLS measurement that provides the hydrodynamic diameter of a hypothetical sphere formed by a diffuse layer (organic molecule layer and solvation ions) surrounding the dispersed MNPs, whereas TEM indicates its precise size [42]. The difference in particle size between these measurements revealed the thickness of the organic layer that acted as a stabilizing agent for MNPs in colloidal solutions [43]. As a result, both CS-AgNPs and CS-AuNPs were stable at normal room conditions for more than three weeks after synthesis.

The TGA and DTA curves of dried CS extract, CS-AgNPs, and CS-AuNPs are shown in Figures 6(a)–6(c), respectively. According to the TGA curves, the thermal behavior of MNPs can be divided into two main stages. In the first stage, at temperatures ranged from room temperature up to 200°C, the initial weight loss of ~8.5% for dried extract, ~14% for AgNPs, and ~15% for AuNPs was observed. This slight weight loss corresponds to the evaporation of physically adsorbed water molecules on the MNP surface and the volatile compounds presented in CS extract [44]. The second stage is the weight loss that occurred in the temperature range up to 610°C. As can be seen, the DTA curves of all samples show only endothermic peaks in the studied temperature range. The significant weight loss in this stage (~72.5% for dried extract, ~29% for AgNPs, and ~53% for AuNPs) was due to the decomposition of phytochemical constituents on the surfaces of MNPs [45]. Thus, the thermal behavior of MNPs confirmed the role of organic phytochemicals from the CS extract in the stabilization of the nanoparticles.

3.3. Catalytic Activity for Reduction of Nitrophenols. Among the nitrophenol family, 2-NP and 3-NP discharged mainly from the production of dyestuffs and fungicides industries are environmental hazards, which can cause methemoglobinemia. Meanwhile, their reduced products (2-AP and 3-AP) are useful chemicals. 2-AP is found in many applications such as photographic developer, corrosion inhibitor in paints, and anticorrosion-lubricating agent in two-cycle engine fuels. 3-AP is commonly used as a precursor to the

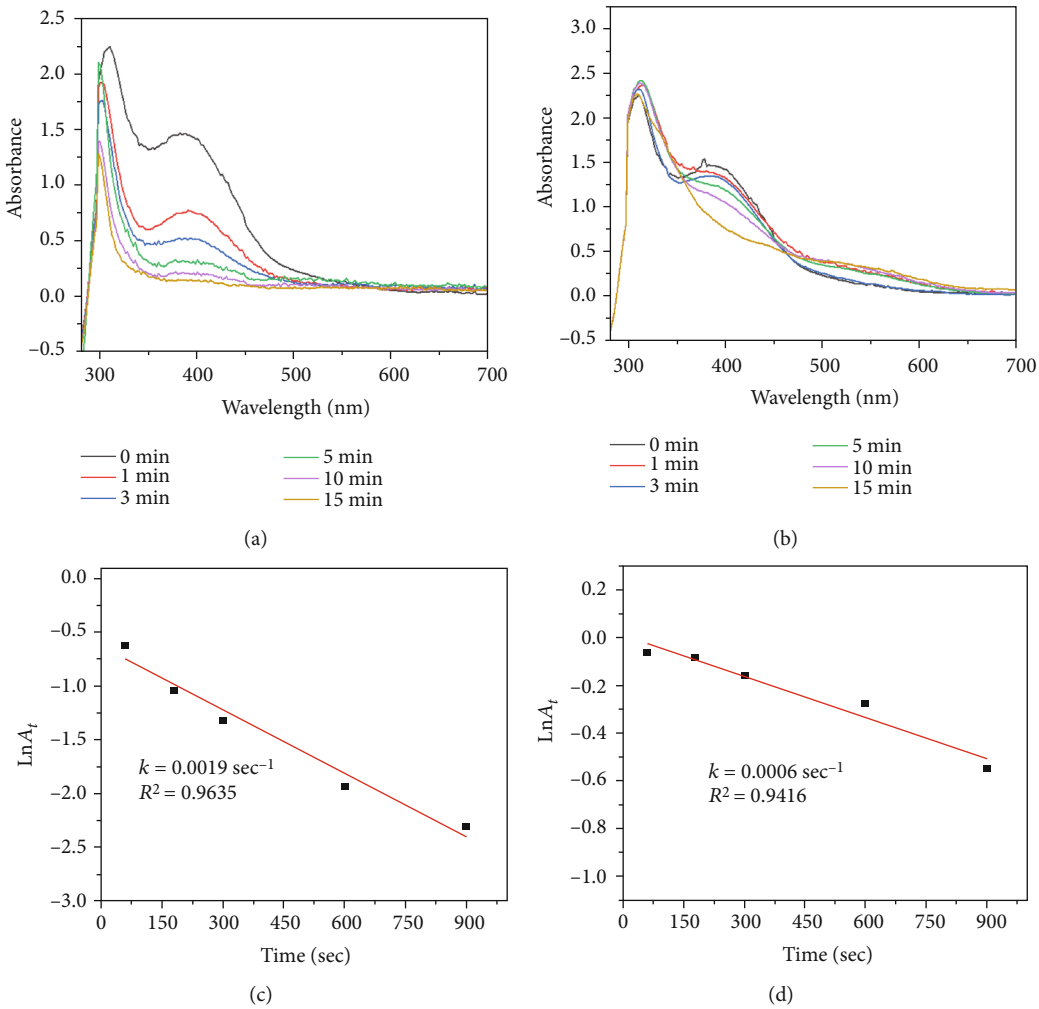

Figure 8: UV-Vis spectra (a, b) and first-order kinetics (c, d) for degradation of 3-NP by $NaBH_4$ in the presence of CS-AgNPs (a, c) and CS-AuNPs (b, d).

preparation of 5-aminosalicylic acid, a drug usually called mesalazine for the treatment of ulcerative colitis [46]. In this study, the catalytic reduction of those nitrophenols by $NaBH_4$ with the biosynthesized MNPs as a catalyst was monitored spectrophotometrically in a cuvette under normal room conditions. A small amount of MNPs was used to avoid the overlap of its SPR band and the UV-Vis spectral band of nitrophenolate ions. In this case, the peak intensity of MNPs is considered negligible compared to those of nitrophenolate ions and can be ignored. The aqueous solution of 2-NP and 3-NP shows characteristic peaks at 410 and 390 nm in the visible region based on the formation of respective nitrophenolate ions in a slightly alkaline medium. The mechanism of catalytic reduction of nitrophenols using $NaBH_4$ and MNPs was described in [44, 47]. In the first step, the adsorption of nitrophenolic molecules occurred on the surface of MNPs. Then, the first-order reaction took place on the catalyst surface, whose rate was proportional to the adsorbed amount of nitrophenols. In the second step, an electron transfer from the donor ($NaBH_4$) to the receptor (nitrophenols) happened at the active sites of MNPs, leading to the formation of respective APs. During the reduction process, the gradual decrease in the optical density at 410 nm for 2-NP and 390 nm for 3-NP was observed (Figures 7(a), 7(b), 8(a), and 8(b)). The reduction rate constant can be determined via the slope of the linear equation $\ln(A_t) = -kt + \ln(A_o)$ (Figures 7(c), 7(d), 8(c), and 8(d)).

As described in Figures 7 and 8, both CS-AgNPs and CS-AuNPs exhibited better catalytic performance toward 2-NP compared to 3-NP. The 2-NP compound could be completely reduced within 15 min ($k = 2.5.10^{-3}$/s) and 10 min ($k = 2.8.10^{-3}$/s) when using CS-AgNPs and CS-AuNPs, respectively. In the case of 3-NP, the degradation almost finished within 11 min ($k = 1.9.10^{-3}$/s) by using CS-AgNPs and within 15 min ($k = 6.0.10^{-4}$/s) for CS-AuNPs. It is noteworthy that the surrounding organic layer could prevent contact between the reactants and the nanoparticles, thereby affecting the catalytic activity. However, this effect could not play a significant role for both CS-AgNPs and CS-AuNPs, since the size of BH_4^- and nitrophenolate ions is relatively small, compared to the size of the organic layer surrounding MNPs. These ions can pass through the gap

Table 1: Comparative reaction rate constants k of the catalytic reduction of 2-NP and 3-NP using AgNPs and AuNPs as catalysts.

Type of NPs	MNPs	Plant	Particle size (nm)	Rate constant (sec^{-1})	References
2-NP	AuNPs	*Lobophora variegata*	2-12	$1.2.10^{-3}$	[40]
	AgNPs	*Codonopsis pilosula*	10	$2.5.10^{-3}$	[41]
	AuNPs		20	$1.2.10^{-3}$	
	AgNPs	Corncob	11	$2.1.10^{-3}$	[48]
	AuNPs		35	$3.0.10^{-3}$	
	AgNPs	*Caulis Spatholobi*	16.4	$2.5.10^{-3}$	This work
	AuNPs		18.2	$2.8.10^{-3}$	
3-NP	AuNPs	*Lobophora variegata*	2-12	$4.5.10^{-3}$	[40]
	AgNPs	Corncob	11	$2.8.10^{-3}$	[48]
	AuNPs		35	$8.0.10^{-3}$	
	AgNPs	*Codonopsis pilosula*	10	$1.7.10^{-3}$	[41]
	AuNPs		20	$4.0.10^{-3}$	
	AgNPs	*Caulis Spatholobi*	16.4	$1.9.10^{-3}$	This work
	AuNPs		18.2	$6.0.10^{-4}$	

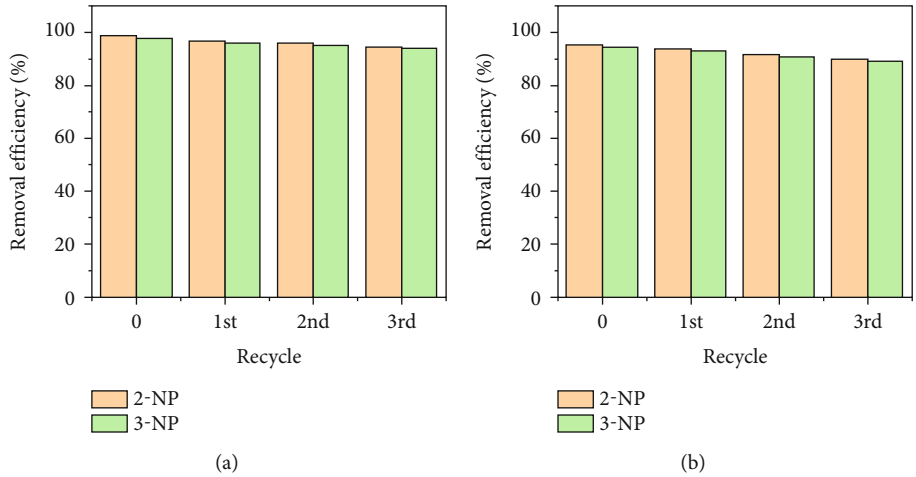

Figure 9: Reusability of CS-AgNPs (a) and CS-AuNPs (b) for 2-NP and 3-NP degradation.

between the organic molecules of the protective layer to contact with the nanoparticles, initiating the catalytic process [43]. In fact, the CS-AgNP and CS-AuNP samples possessed the catalytic activity superior to those of some MNPs biosynthesized by extracts from other plants (Table 1).

For practical applications, the reusability of heterogeneous catalysts is one of the critical factors to enhance the value of the material due to the long-term use and reducing the cost. In this study, the recyclable catalytic performance of MNPs was examined for four recycles of the reduction of 2-NP and 3-NP. The mentioned above procedure was used. After each cycle, MNPs were separated by centrifugation and washed carefully with distilled water and ethanol for the next reuse. As can be seen in Figure 9, the biosynthesized CS-AgNPs and CS-AuNPs possessed almost the same catalytic performance towards both 2-NP and 3-NP after four successive recycles. The yield of about 96% for CS-AgNPs (Figure 9(a)) and 95% for CS-AuNPs (Figure 9(b)) was observed in the last recycle, confirming its excellent recyclability.

4. Conclusions

In this work, a green single-step method for the biofabrication of pure AgNPs and AuNPs without using any expensive reducing and capping agents was reported. Herein, the extract from *Caulis Spatholobi* stems showed its efficacy in both processes of reducing precious metal ions and stabilizing just formed MNPs. The spherical CS-AgNPs and CS-AuNPs with a size range of 10-20 nm were obtained. The biogenic CS-AgNPs and CS-AuNPs exhibited a high catalytic activity toward the degradation of 2-NP and 3-NP. Therefore, the biofabrication method based on *Caulis Spatholobi* extract provides a new opportunity in finding stable metal nanoparticles with enhanced catalytic performance and recyclability.

Data Availability

The data used to support the findings of this study are included within the article.

Conflicts of Interest

The authors declare that they have no conflicts of interest.

References

[1] L. Sherin, A. Sohail, U.-e.-S. Amjad, M. Mustafa, R. Jabeen, and A. Ul-Hamid, "Facile green synthesis of silver nanoparticles using _Terminalia bellerica_ kernel extract for catalytic reduction of anthropogenic water pollutants," *Colloid and Interface Science Communications*, vol. 37, p. 100276, 2020.

[2] S. B. Parit, V. C. Karade, R. B. Patil et al., "Bioinspired synthesis of multifunctional silver nanoparticles for enhanced antimicrobial and catalytic applications with tailored SPR properties," *Mater. Today Chem.*, vol. 17, p. 100285, 2020.

[3] A. Bala and G. Rani, "A review on phytosynthesis, affecting factors and characterization techniques of silver nanoparticles designed by green approach," *Int. Nano Lett.*, vol. 10, no. 3, pp. 159–176, 2020.

[4] F. Esmaile, H. Koohestani, and H. Abdollah-Pour, "Characterization and antibacterial activity of silver nanoparticles green synthesized using _Ziziphora clinopodioides_ extract," *Environmental Nanotechnology, Monitoring & Management*, vol. 14, p. 100303, 2020.

[5] N. Cyril, J. B. George, P. V. Nair et al., "Catalytic activity of _Derris trifoliata_ stabilized gold and silver nanoparticles in the reduction of isomers of nitrophenol and azo violet," *Nano-Structures and Nano-Objects*, vol. 22, p. 100430, 2020.

[6] J. L. Gardea-Torresdey, E. Gomez, J. R. Peralta-Videa, J. G. Parsons, H. Troiani, and M. Jose-Yacaman, "Alfalfa sprouts: a natural source for the synthesis of silver nanoparticles," *Langmuir*, vol. 19, no. 4, pp. 1357–1361, 2003.

[7] P. Velmurugan, M. Cho, S. S. Lim et al., "Phytosynthesis of silver nanoparticles by Prunus yedoensis leaf extract and their antimicrobial activity," *Materials Letters*, vol. 138, pp. 272–275, 2015.

[8] L. K. Ruddaraju, P. N. V. K. Pallela, S. V. N. Pammi, V. S. Padavala, and V. R. M. Kolapalli, "Synergetic antibacterial and anticarcinogenic effects of Annona squamosa leaf extract mediated silver nano particles," *Materials Science in Semiconductor Processing*, vol. 100, pp. 301–309, 2019.

[9] T. T.-N. Nguyen, T.-T. Vo, B. N.-H. Nguyen et al., "Silver and gold nanoparticles biosynthesized by aqueous extract of burdock root, Arctium lappa as antimicrobial agent and catalyst for degradation of pollutants," *Journal of Analytical Science and Technology*, vol. 25, no. 34, pp. 34247–34261, 2018.

[10] T. Ahmad, A. N. Veenu, U. Farooq et al., "Biosynthesis, characterization and photo-catalytic degradation of methylene blue using silver nanoparticles," *Materials Today: Proceedings*, vol. 29, pp. 1039–1043, 2020.

[11] F. Ameen, P. Srinivasan, T. Selvankumar et al., "Phytosynthesis of silver nanoparticles using Mangifera indica flower extract as bioreductant and their broad-spectrum antibacterial activity," *Bioorganic Chemistry*, vol. 88, p. 102970, 2019.

[12] N. Kumaresan, M. M. A. Sinthiya, K. Ramamurthi, R. Ramesh Babu, and K. Sethuraman, "Visible light driven photocatalytic activity of ZnO/CuO nanocomposites coupled with rGO heterostructures synthesized by solid-state method for RhB dye degradation," *Arabian Journal of Chemistry*, vol. 13, no. 2, pp. 3910–3928, 2020.

[13] G. Rajakumar, T. Gomathi, M. Thiruvengadam, V. Devi Rajeswari, V. N. Kalpana, and I. M. Chung, "Evaluation of anti-cholinesterase, antibacterial and cytotoxic activities of green synthesized silver nanoparticles using from Millettia pinnata flower extract," *Microbial Pathogenesis*, vol. 103, pp. 123–128, 2017.

[14] V. K. M. Katta and R. S. Dubey, "Green synthesis of silver nanoparticles using Tagetes erecta plant and investigation of their structural, optical, chemical and morphological properties," *Materials Today: Proceedings*, 2020.

[15] W. K. A. W. M. Khalir, K. Shameli, S. D. Jazayeri, N. A. Othman, N. W. C. Jusoh, and N. M. Hassan, "Biosynthesized silver nanoparticles by aqueous stem extract of Entada spiralis and screening of their biomedical activity," *Frontiers in Chemistry*, vol. 8, 2020.

[16] P. Karthiga, "Preparation of silver nanoparticles by _Garcinia mangostana_ stem extract and investigation of the antimicrobial properties," *Biotechnology Research and Innovation*, vol. 2, no. 1, pp. 30–36, 2018.

[17] I. M. Chung, I. Park, K. Seung-Hyun, M. Thiruvengadam, and G. Rajakumar, "Plant-mediated synthesis of silver nanoparticles: their characteristic properties and therapeutic applications," *Nanoscale Research Letters*, vol. 11, no. 1, 2016.

[18] K. Paulkumar, G. Gnanajobitha, M. Vanaja et al., "Piper nigrum leaf and stem assisted green synthesis of silver nanoparticles and evaluation of its antibacterial activity against agricultural plant pathogens," *Scientific World Journal*, vol. 2014, pp. 1–9, 2014.

[19] D. Kalaiselvi, A. Mohankumar, G. Shanmugam, S. Nivitha, and P. Sundararaj, "Green synthesis of silver nanoparticles using latex extract of Euphorbia tirucalli: a novel approach for the management of root knot nematode, Meloidogyne incognita," *Crop Protection*, vol. 117, pp. 108–114, 2019.

[20] C. Rajkuberan, S. Prabukumar, G. Sathishkumar, A. Wilson, K. Ravindran, and S. Sivaramakrishnan, "Facile synthesis of silver nanoparticles using _Euphorbia antiquorum_ L. latex extract and evaluation of their biomedical perspectives as anticancer agents," *Journal of Saudi Chemical Society*, vol. 21, no. 8, pp. 911–919, 2017.

[21] W. M. Salem, M. Haridy, W. F. Sayed, and N. H. Hassan, "Antibacterial activity of silver nanoparticles synthesized from latex and leaf extract of Ficus sycomorus," *Industrial Crops and Products*, vol. 62, pp. 228–234, 2014.

[22] S. Dangi, A. Gupta, D. K. Gupta, S. Singh, and N. Parajuli, "Green synthesis of silver nanoparticles using aqueous root extract of _Berberis asiatica_ and evaluation of their antibacterial activity," *Chemical Data Collections*, vol. 28, p. 100411, 2020.

[23] J. Xue, T. Liu, Y. Liu et al., "Neuroprotective effect of biosynthesised gold nanoparticles synthesised from root extract of Paeonia moutan against Parkinson disease – in vitro & in vivo model," *Journal of Photochemistry and Photobiology B: Biology*, vol. 200, p. 111635, 2019.

[24] B. Akilandaeaswari and K. Muthu, "Green method for synthesis and characterization of gold nanoparticles using Lawsonia inermis seed extract and their photocatalytic activity," *Materials Letters*, vol. 277, p. 128344, 2020.

[25] M. S. Mohseni, M. A. Khalilzadeh, M. Mohseni et al., "Green synthesis of Ag nanoparticles from pomegranate seeds extract and synthesis of Ag-starch nanocomposite and characterization of mechanical properties of the films," *Biocatalysis and Agricultural Biotechnology*, vol. 25, p. 101569, 2020.

[26] B. Ajitha, Y. A. K. Reddy, and P. S. Reddy, "Biogenic nanoscale silver particles by _Tephrosia purpurea_ leaf extract and their inborn antimicrobial activity," *Spectrochimica Acta Part A: Molecular and Biomolecular Spectroscopy*, vol. 121, pp. 164–172, 2014.

[27] L. Sun, Q. Li, Y. Guo et al., "Extract of _Caulis Spatholobi_ , a novel platelet inhibitor,efficiently suppresses metastasis of colorectal cancer by targeting tumor cell-induced platelet aggregation," *Biomedicine & Pharmacotherapy*, vol. 123, p. 109718, 2020.

[28] X. Chen, Q. Li, X.-X. Kan et al., "Extract of Caulis Spatholobi, a novel blocker targeting tumor cell-induced platelet aggregation, inhibits breast cancer metastasis," *Oncology Reports*, vol. 36, no. 6, pp. 3215–3224, 2016.

[29] H. Wagner, R. Bauer, and D. Melchart, *Chromatographic Fingerprint Analysis of Herbal Medicines*, Springer-Verlag Wien, Germany, 2011.

[30] C. Vijilvani, M. R. Bindhu, F. C. Frincy et al., "Antimicrobial and catalytic activities of biosynthesized gold, silver and palladium nanoparticles from Solanum nigurum leaves," *Journal of Photochemistry and Photobiology B: Biology*, vol. 202, p. 111713, 2020.

[31] V. M. Kariuki, I. Yazgan, A. Akgul, A. Kowal, M. Parlinska, and O. A. Sadik, "Synthesis and catalytic, antimicrobial and cytotoxicity evaluation of gold and silver nanoparticles using biodegradable, *IT*-conjugated polyamic acid," *Environmental Science. Nano*, vol. 2, no. 5, pp. 518–527, 2015.

[32] T. M. T. Nguyen, T. T. T. Huynh, C. H. Dang et al., "Novel biogenic silver nanoparticles used for antibacterial effect and catalytic degradation of contaminants," *Research on Chemical Intermediates*, vol. 46, no. 3, pp. 1975–1990, 2020.

[33] A. Chhatre, P. Solasa, S. Sakle, R. Thaokar, and A. Mehra, "Color and surface plasmon effects in nanoparticle systems: case of silver nanoparticles prepared by microemulsion route," *Colloids and Surfaces A: Physicochemical and Engineering Aspects*, vol. 404, pp. 83–92, 2012.

[34] A. Liang, Q. Liu, G. Wen, and Z. Jiang, "The surface-plasmon-resonance effect of nanogold/silver and its analytical applications," *TrAC Trends in Analytical Chemistry*, vol. 37, pp. 32–47, 2012.

[35] A. Gangula, R. Podila, M. Ramakrishna, L. Karanam, C. Janardhana, and A. M. Rao, "Catalytic reduction of 4-nitrophenol using biogenic gold and silver nanoparticles derived from Breynia rhamnoides," *Langmuir*, vol. 27, no. 24, pp. 15268–15274, 2011.

[36] M. Behravan, A. Hossein Panahi, A. Naghizadeh, M. Ziaee, R. Mahdavi, and A. Mirzapour, "Facile green synthesis of silver nanoparticles using Berberis vulgaris leaf and root aqueous extract and its antibacterial activity," *International Journal of Biological Macromolecules*, vol. 124, pp. 148–154, 2019.

[37] M. J. Maleki, M. Pourhassan-Moghaddam, A. Karimi, A. Akbarzadeh, N. Zarghami, and S. A. Mohammadi, "Synthesis, characterisation, and application of chamomile gold nanoparticles in molecular diagnostics: a new component for PCR kits," *Biointerface Res. Appl. Chem.*, vol. 9, no. 6, pp. 4635–4641, 2019.

[38] Y. H. Yang, X. Z. Li, and S. Zhang, "Preparation methods and release kinetics of Litsea cubeba essential oil microcapsules," *RSC Advances*, vol. 8, no. 52, pp. 29980–29987, 2018.

[39] K. X. Lee, K. Shameli, M. Miyake et al., "Green synthesis of gold nanoparticles using aqueous extract of Garcinia mangostana fruit peels," *Journal of Nanomaterials*, vol. 2016, 7 pages, 2016.

[40] P. Kaithavelikkakath Francis, S. Sivadasan, A. Avarachan, and A. Gopinath, "A novel green synthesis of gold nanoparticles using seaweedLobophora variegataand its potential application in the reduction of nitrophenols," *Particulate Science and Technology*, vol. 38, no. 3, pp. 365–370, 2020.

[41] V. D. Doan, B. A. Huynh, T. D. Nguyen et al., "Biosynthesis of silver and gold nanoparticles using aqueous extract of Codonopsis pilosula roots for antibacterial and catalytic applications," *Journal of Nanomaterials*, vol. 2020, 18 pages, 2020.

[42] B. Laban, U. Ralević, S. Petrović et al., "Green synthesis and characterization of nontoxic L-methionine capped silver and gold nanoparticles," *Journal of Inorganic Biochemistry*, vol. 204, p. 110958, 2020.

[43] V. D. Doan, A. T. Thieu, T. D. Nguyen et al., "Biosynthesis of gold nanoparticles using Litsea cubeba fruit extract for catalytic reduction of 4-nitrophenol," *Journal of Nanomaterials*, vol. 2020, 10 pages, 2020.

[44] S. S. Royji Albeladi, M. A. Malik, and S. A. Al-thabaiti, "Facile biofabrication of silver nanoparticles using Salvia officinalis leaf extract and its catalytic activity towards Congo red dye degradation," *Journal of Materials Research and Technology*, vol. 9, no. 5, pp. 10031–10044, 2020.

[45] T. T. Vo, C. H. Dang, V. D. Doan, V. S. Dang, and T. D. Nguyen, "Biogenic synthesis of silver and gold nanoparticles from Lactuca indica leaf extract and their application in catalytic degradation of toxic compounds," *Journal of Inorganic and Organometallic Polymers and Materials*, vol. 30, no. 2, pp. 388–399, 2020.

[46] Z. Xiong, H. Zhang, W. Zhang, B. Lai, and G. Yao, "Removal of nitrophenols and their derivatives by chemical redox: a review," *Chemical Engineering Journal*, vol. 359, pp. 13–31, 2019.

[47] Y. Cui, X. Guo, X. Lai et al., "Green synthesis of jujube-polysaccharide-stabilized gold nanoparticles for reduction of 4-nitrophenol," *Chemistry Select.*, vol. 4, no. 39, pp. 11483–11487, 2019.

[48] V.-D. Doan, V.-S. Luc, T. L.-H. Nguyen, T.-D. Nguyen, and T.-D. Nguyen, "Utilizing waste corn-cob in biosynthesis of noble metallic nanoparticles for antibacterial effect and catalytic degradation of contaminants," *Environmental Science and Pollution Research*, vol. 27, no. 6, pp. 6148–6162, 2020.